 doi:10.20944/preprints201711.0064.v1

Article

Influence of Nanoscaled Surface Modification on the Reaction of Al/Ni Multilayers

Heike Bartsch [1,*], José Manuel Mánuel [2,3] and Rolf Grieseler [1,4]

[1] Technische Universität Ilmenau, Institute for Micro- and Nanotechnologies, MacroNano®, 98693 Ilmenau, Germany; heike.bartsch@tu-ilmenau.de
[2] Universidad de Cádiz, Facultad de Ciencias, 11510 Puerto Real, Spain; jose.manuel@uca.es
[3] IMEYMAT: Institute of Research on Electron Microscopy and Materials of the University of Cádiz, Spain.
[4] Pontificia Universidad Católica del Perú, San Miguel-32 Lima
* Correspondence: heike.bartsch@tu-ilmenau.de; Tel.: +49-3677-69-3452

Abstract: Sputtered reactive multilayers applied as a heat source in electronic joining processes are an emerging technology. It promises low-stress assembly of components while improving the thermal contact and thus thermal resistance. The use of nanostructures can significantly enhance the adhesion and reliability of joints between different materials. This work presents a phenomenological proof of the hypothesis. Reactive multilayers of nickel and aluminum directly deposited on nanostructured surfaces of silicon wafers and reference samples with flat surface are compared. The investigation of the self-propagating reaction shows a clear influence of the layer thickness, dependent on the multilayer thickness and nanostructure morphology. Rapid thermal annealing results in the formation of $Al_{1.1}Ni_{0.9}$ phase. The necessary annealing temperature is much higher than this applied for nanofoils, sputtered multilayer or particles. The nanostructured interface seems to hinder the full transformation of the present nickel. On the other hand, the surfaces modification improves adhesion of the formed alloy on silicon surfaces and can thus increase the reliability of joints based on reactive aluminum/nickel multilayer. The use of nanostructured surface modifications is thus a promising approach to realized reliable multi-material joints in complex systems.

Keywords: sputtered reactive multilayer; silicon bonding; self-propagating reaction; semiconductor packaging; black silicon; joining technology; energetic material; reactive nanomaterial

1. Introduction

Resource efficient manufacturing requires the development of joining technologies for the assembly of multi-material systems. The use of reactive nanofoils is an emerging technology for the fusion of dissimilar materials. Local heat release can be exploited for stress-reduced joining of materials with high thermal expansion mismatch in microsystems [1]. The assembly of electronic systems with high packaging density and the heat management of such systems is an ongoing challenged for a smart system integration. Sputtered multilayer on ceramic packages can be used for the direct bonding with heat sinks and the immanent roughness of the ceramic surface leads to better adhesion of the sputtered layers in comparison to flat silicon nitride surfaces [2]. The assembly of silicon chips on heat spreaders with excellent thermal contact at low stress is still a challenge of electronic systems integration. The direct deposition of reactive multilayers on silicon chips and their application as well-portioned heat source for chip bonding is a promising approach for low-stress chip mounting on manifold circuit carriers. The positive influence of nanostructures on the strength of ceramic-silicon bonds was shown [3]. This work gives a first view of the interplay between nanostructured interface, reactive multilayer thickness and multilayer growth and their influences on phase forming and reaction propagation using a phenomenological approach.

Preprints (www.preprints.org) | NOT PEER-REVIEWED | Posted: 10 November 2017 doi:10.20944/preprints201711.0064.v1

2. Materials and Methods

Black silicon is produced using p-doped (111) wafer. Nanostructure etching is performed in an Oxford RIE reactor with a pressure of 100 mTorr, working at a power of 100 W and 20°C with helium backing, using a gas flow of 84 sccm SF6, and 66 sccm O2. The process was maintained during 30 minutes, resulting in needles of approximately 1.0 µm of length. A flat wafer without nanostructures is used for comparison purpose. Aluminum/nickel multilayers with a bilayer layer thickness of 50 nm were deposited by magnetron sputtering on the wafer surface. The process was carried out using a cluster system (CS400 by ARDENNE) with a sputtering power of 200 W and a working pressure of $5 \cdot 10^{-3}$ mbar with 80 sccm argon flow and without substrate heating. The obtained deposition rate was 0.32 nm/s for the aluminum and 0.26 nm/s for the nickel. The total thickness varies between 250 nm and 5 µm.

The prepared wafers are broken in samples with an edge length between 1 and 2 cm. The layer morphology on the nanostructures was investigated by SEM (Field-Effect ZEISS Gemini SEM 500 working at 1.5 kV) and TEM (TECNAI S20 working at 200 kV). Single needles were separated by scratching from the substrate and deposited on holey-carbon grids, for the TEM measurements. The images of SEM and TEM analysis are depicted in Figure 1. One sample of each wafer was ignited by electric spark and a platinum electrode, applying a voltage of 50 V and a maximum current of 50 mA with a lab power supply. 50 ignition points were generated and their dimensions were investigated with a microscope in order to assess the influenced region dependent on multilayer thickness on an adequate confidence level. Further samples of each wafer were annealed in a rapid thermal treatment reactor. The maximum temperature T_{max} was varied between 350°C and 550°C. The treated samples were investigated with XRD (Bruker D5000 diffractometer with Göbel mirror, working in Bragg-Brentano mode) to identify formed phase and grade of phase formation.

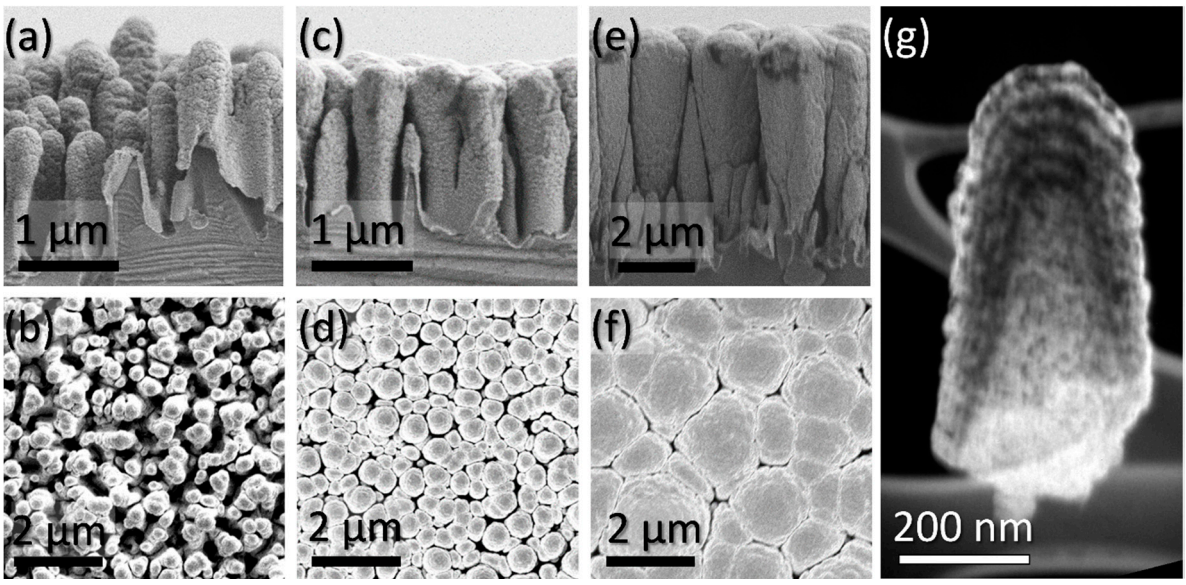

Figure 1. SEM micrographs of multilayers with different thickness, grown on black silicon nanostructures: a), c), e) cross section of thick multilayers with 500 nm, 1 µm and 5 µm thickness; b), d), f) top view on the respective layer; g) Dark Field TEM image of a nanostructure tip with 20 nm radius, coated with a 250-nm-thick multilayer.

3. Results

3.1 Multilayer morphology on nanostructures

The cross sections in Figure 1 a), c) and d) illustrate that the edge coverage of the sputtering process is not uniform. This leads to a progressive growth of larger clusters at the expense of smaller ones. With increasing thickness, the gaps between single nanostructures are filled from the top of the substrate. While single structures covered with a 500-nm-thick multilayer still are separated, some

Preprints (www.preprints.org) | NOT PEER-REVIEWED | Posted: 10 November 2017 doi:10.20944/preprints201711.0064.v1

are touching at the top when the layer is 1 µm thick. The sample covered with a 5-µm-thick layer shows a dense structure with direct contact between single regions on top, but the cross sections indicates that hollows are present at deeper levels. The TEM image in Figure 1 g) makes clear that the deposition rate at the nanostructure´s foot is much lower than on top, resulting in a steady decrease of the bilayer thickness. At a depth of approx. 500 nm from the top of the structure, the bilayer thickness is only ¼ of this on the structure top. It is possible that the intermixed layer thickness and pure metal layers reaches similar thickness at the structure foot. Probably, the crystal structure, grain boundary structure and lattice structure are strongly disrupted in this region.

3.2 Spark ignition

The radius of the effected zone as function of the Al/Ni multilayer thickness is depicted in Figure 2 a). The values follow a Gaussian distribution. Mean values correspond to 84 µm for 500 nm Al/Ni multilayer thickness, 92 µm for 1 µm and 400 µm for 5 µm. The shape of the influenced area is depicted in Figure 2 b) and c). The influenced zone of 5 µm-thick-layers (not depicted) and 500 nm thick layers are characterized by a round contour. The area between molten material and unaffected structures amounts to 100 µm for 5-µm-thick layers. In the case of 500-nm-thick layers it is restricted to 10 µm, approximately. Details of this transition area are depicted in Figure 2 d and e). While the structures in the near vicinity still show closed molten links to the spark area, those next to them are characterized by a changed morphology, but not linked with adjacent ones. Samples with 1-µm-thick Al/Ni multilayers are characterized by a dendrite shape of the effected zone. The reaction propagates along paths and peters out. The contour is irregular and this is the reason for the large variation of the measured distribution in Figure 2 a).

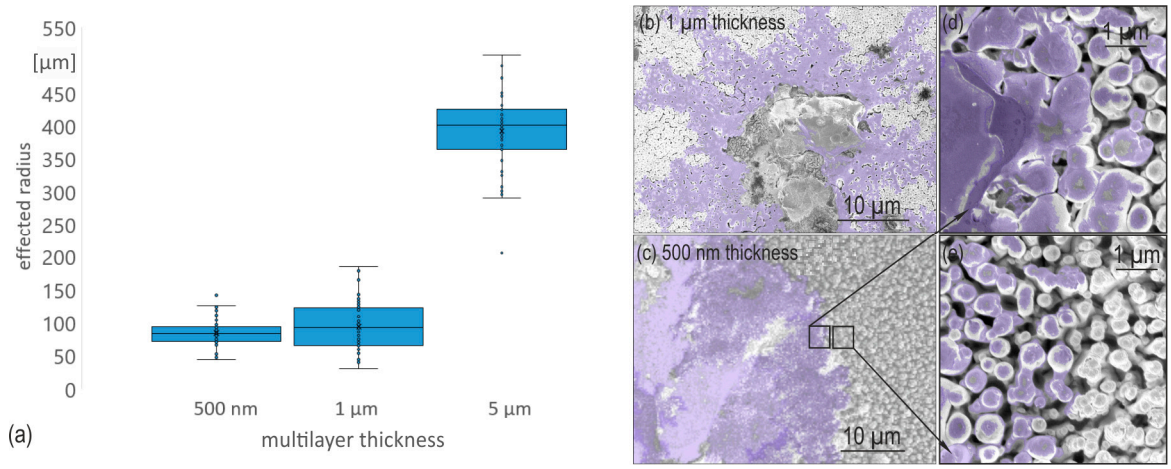

Figure 2. Effected zone dependent on layer thickness. (a) box plot of the effected radius measured by light microscope as function of layer thickness; (b) false color SEM image of ignition zone; zone is minimal larger and has dendrite shape, form is irregular, fractal distribution of the ignition over nanostructures on top, molten areas are colored (c) false color SEM image of 500 nm layer. Ignited zone has a round shape, molten area ends abruptly (d) detail of the border area, molten layers on top are depicted in false color (e) outermost area of influenced zone, some tips show molten structure (false color).

3.3 Rapid thermal annealing

The reactor setup and the annealing profile are depicted in Figure 3. The annealing is carried out under argon atmosphere with a rapid thermal annealing (RTA) furnace (Jet First, Joint Industrial Processor for Electronics). Figure 4 shows the samples treated at 450°C after processing. The layer on

Preprints (www.preprints.org) | NOT PEER-REVIEWED | Posted: 10 November 2017 doi:10.20944/preprints201711.0064.v1

the flat silicon substrate is fully peeled off. This fact was observed for all trials. The adhesion of all layers deposited on nanostructures is excellent.

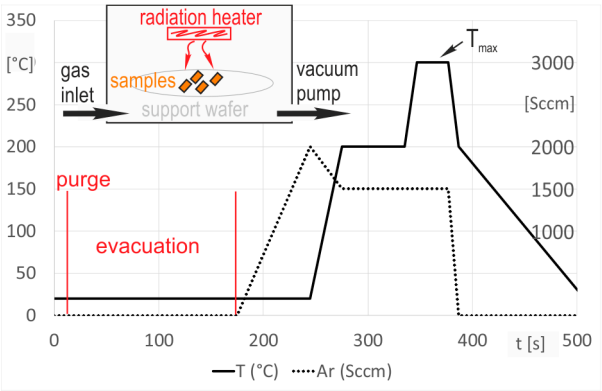

Figure 3. Rapid thermal annealing (RTA) set-up and annealing profile. T_{max} varies between 350°C and 550°C.

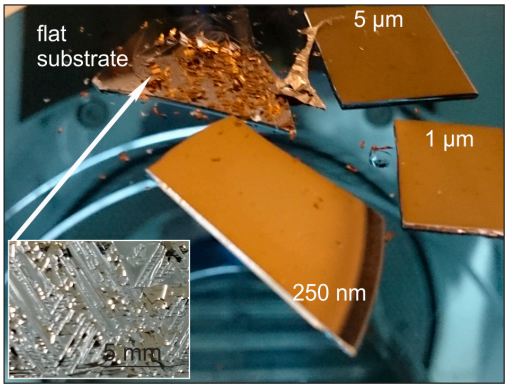

Figure 4. Samples after RTA at 450°C and micrograph of the flat wafer surface.

XRD curves are depicted in Figure 5. Before ignition, peaks for Al and Ni are present. After annealing all Al peaks disappear, and the $Al_{1.1}Ni_{0.9}$ phase arises. However, all samples still present Ni peaks. The relation between the peak intensity was calculated and depicted in a diagram in order to visualize the effects of temperature and multilayer thickness.

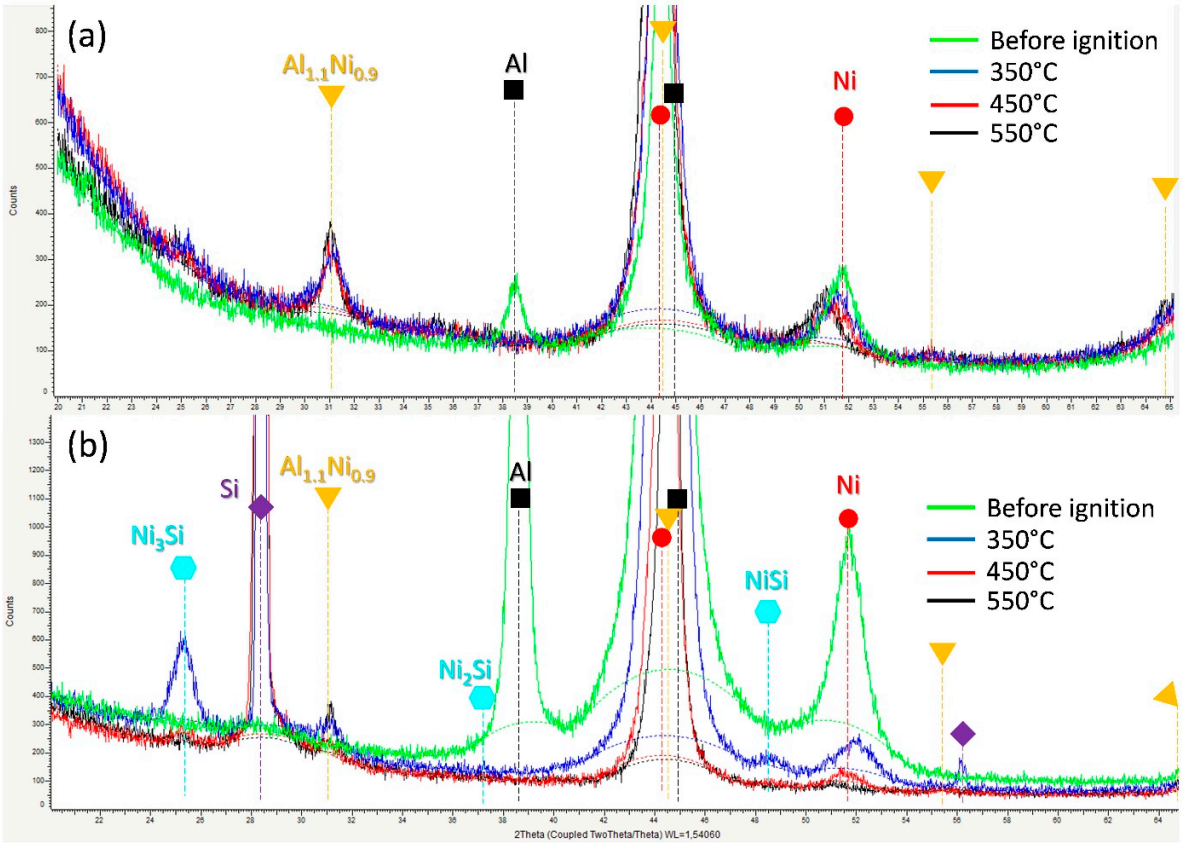

Figure 5. XRD Theta-2Theta curve for (a) samples with 1 µm multilayer, and (b) reference samples (flat wafer with 1 µm multilayer thickness) for RTA at different temperatures.

Preprints (www.preprints.org) | NOT PEER-REVIEWED | Posted: 10 November 2017 doi:10.20944/preprints201711.0064.v1

The phase $Al_{1.1}Ni_{0.9}$ was identified in all XRD measurements. It is formed independently from surface modification and layer thickness. This phase is characterized by an excess of Al. Peaks of metallic Ni were found on all nanostructured samples in Figure 5 (a). The annealed layer on the flat reference wafer show additional peaks, indicating the presence of Ni/Si alloys with a strong intensity at 350°C. The nickel peak decreases on flat wafers with T_{max} and disappears totally at T_{max}=550°. The intensities of selected peaks are used as markers for the relation of present metal and alloy portions. The relative intensity I_{relM} of the respective metal is calculated using Equation 1. The index M stands for Al= aluminum, Ni= nickel and AlNi= $Al_{1.1}Ni_{0.9}$ alloy. The intensities I_{Al}, I_{Ni} and I_{NiAl} are extracted from fitted curves of the respective measurement.

$$I_{relM} = \frac{I_M}{I_{Al}+I_{Ni}+I_{AlNi}} \times 100\% \quad (1)$$

The obtained relative intensities I_{relM} for all measurements carried out at 350°C are depicted in Figure **6**. Figure 7 compares the relative intensity of the $Al_{1.1}Ni_{0.9}$ peak for multilayer thickness 1 µm and 5 µm with the values of 1-µm-thick multilayer on the flat reference wafer.

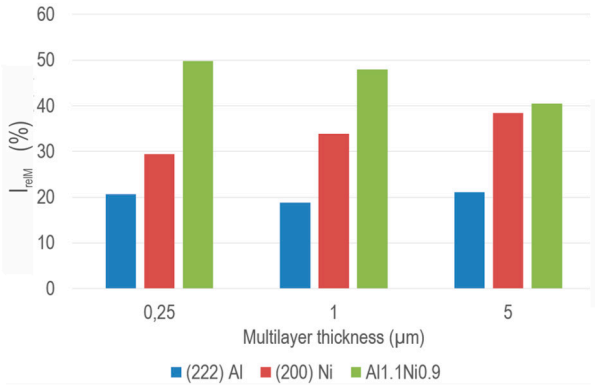

Figure 6. Relation between the intensities of selected peaks as marker for Al, Ni and $Al_{1.1}Ni_{0.9}$ content after RTA treatment at 350°C

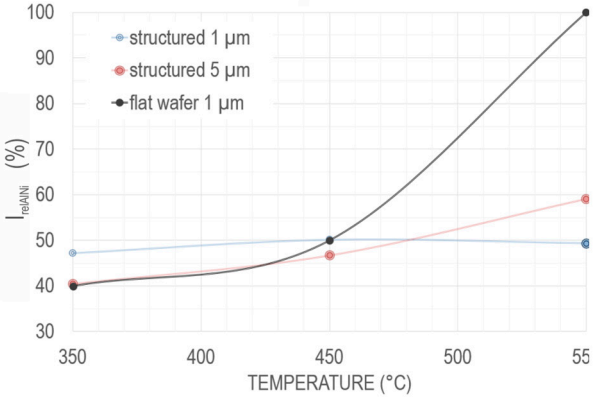

Figure 7. Relative intensity I_{AlNi} for total thickness of 1 µm and 5 µm compared with 1-µm-thick layer on flat reference wafer.

4. Discussion

4.1 Self-propagation of the reaction front

Spark ignition starts a self-propagating reaction. The propagation peters out depending on the amount of dissipated heat and reaction enthalpy, which is released during the exothermic process. Reaction enthalpy and propagation velocity depend on bilayer thickness and width of the intermixed layer [4]. Tests with nanofoils have shown, that both decrease with increasing surface waviness of thick sputtered layers [4]. The authors attribute the effect to stacking faults and a decreasing efficiency of the chemical chain reaction linked to that fact. They observed the propagation of a reaction front on nanofoils initiated on a point with high-speed videometry. The front propagates in a circular way. The same circular propagation was observed on our samples with layer thickness of 500 nm and 5 µm as illustrated in Figure 2. However, the ignition on 1-µm-thick layers propagates in an irregular shape, characterized by a star-shape. The different results have its origin in different heat and mass transport conditions. It manifests in the size of the effected zone depicted in Figure 2 a). Thin layers have a low cross section, the mass transport by diffusion is therefore limited and the reactive front propagates mainly by the heat distribution over the substrate. The released energy is low in comparison to the dissipated heat. Therefore, only small circular regions are transformed and the zone ends abruptly. Between molten and unaffected structures only lie few micrometers, as demonstrated in Figure 2 d), e). The samples with 1 µm thick layers on nanostructures show an only slightly higher radius of the effected zone (Figure 2 a). Reaction paths form dendrites, which peter

Preprints (www.preprints.org) | NOT PEER-REVIEWED | Posted: 10 November 2017 doi:10.20944/preprints201711.0064.v1

out (see Figure 2 b). The top view on the layer, Figure 1 d), illustrates that some nanostructures are in close contact on the tips. The combustion front can propagate here along the tips fostered by a diffusion driven phase formation reaction. At the groves, the thin layers have only a small contact cross section. The dependency between contact area and propagation velocity was demonstrated in [5]. Even if the thermal contact is perfect, the reduced contact area on the nanostructures foot hinders a rapid propagation. The heat dissipation provokes thus the petering out of the reaction. Thick layers with a thickness of 5 µm have a dense contact at the structure tip. This enables diffusion along the layer top, enhancing propagation. The significant increase of the effected zone is attributed to the thicker layer contributing to a higher heat release. The denser morphology, coupled with less grain boundary disorders, can be an additional effect contributing to a better reaction efficiency.

4.2 Rapid thermal annealing tests

The comparison of the relative peak intensity I_{relM} in Figure 6 demonstrates that the annealing temperature of 350°C is too low to achieve a complete transformation. The necessary annealing temperature is thus much higher the expected one for foils or particles [6], which is significantly below 300°C for bilayer thickness smaller than 100 nm. The decreasing portion of $Al_{1.1}Ni_{0.9}$ alloy with increasing layer thickness indicates a diffusion limited process, where no exothermic heat is released.

An increase of the temperature up to 550°C (Figure 7) does not lead to a complete transformation if the layers are sputtered on nanostructures. In comparison, 1-µm-thick multilayers can be completely transformed if they are applied on flat silicon. The occurring SiNi phases (Figure 5 b) could not be found on the nanostructured samples (Figure 5 a). This might be owed to the penetration depth of the X-ray measurement, which might hinder the detection of occurring similar phases at the nanostructured interface on the backside of the well adhered layers on these samples. However, on all nanostructures samples the nickel peak is present, while it decreases on flat samples with increasing temperature and disappears totally at 550°C. An investigation of the diffusion, based on rapid thermal annealed samples, has shown that grain boundary diffusion dominates the behavior of the sputtered Al/Ni bilayers [7]. The deviation of nickel excess observed between nanostructured and flat substrates in this study is assigned to increased surface to volume ratio of nanostructures, which is paired with different crystal structure and grain size due to energetic conditions at the small radius, especially at concave structures, where the bilayer thickness is additionally extremely thin (compare Figure 1 g). The single layer thickness in this region reaches the magnitude of the intermixed zone. Although the influence of the relation between bilayer thickness and thickness of the intermixing zone is investigated for Al/Ni nanofoils [4], its influence cannot be estimated for such thin layers applied on structures in the nanoscale.

5. Conclusions

The propagation of the reaction front is driven by thermal conductivity when layers are thin. Emerging direct contact of the coated structure tips with increasing layer thickness fosters diffusion driven mass transport and propagation along the nanostructures tip. Figure 8 illustrates the propagation along thin layers and thick layers on nanostructures schematically. A detailed study of the influences on microstructure level is necessary to identify crucial parameters.

Rapid thermal annealing test have shown that nanostructured surfaces improve adhesion of the reactive layers on silicon surfaces and can thus reduce the strength of joints based on reactive aluminum/nickel

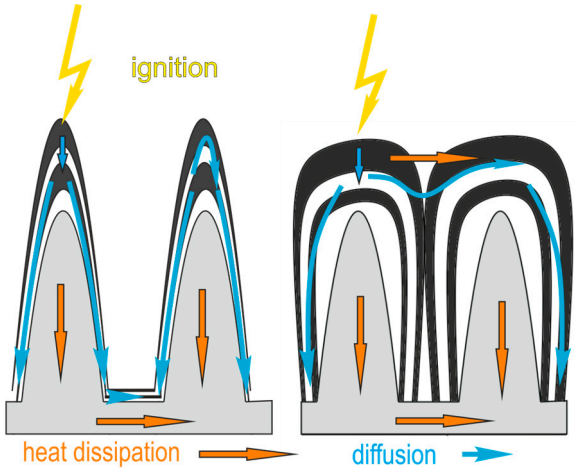

Figure 8. Schematic illustration of the mass and heat transport for thin and thick multilayers.

multilayer. The use of nanostructured surface modifications is thus a promising approach to realized reliable multi-material joints in complex systems.

Acknowledgments: The authors acknowledge for the support from the Alexander von Humboldt Foundation, through the "Humboldt Research Fellowship for Postdoctoral Researchers Programme" (Ref. 3.3-1 1S8421-ES-HFST-P). A special thank goes to Prof. Jens Müller for supervising this exchange. Further, the authors would express deep thankfulness to Prof. Peter Schaaf who enabled the sound cooperation among all staff of the material science department of IMN MacroNano® and the authors as base for this study.

Author Contributions: Heike Bartsch designed the experiments, performed the experiments, interpreted the results and wrote the paper. José Manuel Mánuel performed SEM and TEM studies, carried out XRD measurements and analyzed the respective data. Rolf Grieseler conceived the experiment and provided his experience of reactive multilayer processing and analysis. He supported the methodology concept and discussion section.

Conflicts of Interest: The authors declare no conflict of interest.

References

1. Welker, T.; Geiling, T.; Bartsch, H.; Müller, J. Design and Fabrication of Transparent and Gas-Tight Optical Windows in Low-Temperature Co-Fired Ceramics. *Int. J. Appl. Ceram. Technol.* **2013**, *10*, 405–412, doi:10.1111/ijac.12034.
2. Grieseler, R.; Welker, T.; Müller, J.; Schaaf, P. Bonding of low temperature co-fired ceramics to copper and to ceramic blocks by reactive aluminum/nickel multilayers. *physica status solidi (a)* **2012**, *209, doi:*10.1002/pssa.201127470.
3. Fischer, M.; Bartsch, H.; Pawlowski, B.; Gade, R.; Barth, S.; Mach, M.; Stubenrauch, M.; Hoffmann, M.; Müller, J. Silicon on Ceramics - A New Integration Concept for Silicon Devices to LTCC. *Journal of microelectronics and electronic packaging* **2009**, 1–5.
4. Theodossiadis, G.D.; Zaeh, M.F. Study of the kinetic and energetic reaction properties of multilayered aluminum–nickel nanofoils. *Prod. Eng. Res. Devel.* **2017**, *11*, 245–253, doi:10.1007/s11740-017-0733-8.
5. Sraj, I.; Vohra, M.; Alawieh, L.; Weihs, T.P.; Knio, O.M. Self-Propagating Reactive Fronts in Compacts of Multilayered Particles. *Journal of Nanomaterials* **2013**, *2013*, 1–11, doi:10.1155/2013/198096.
6. Fritz, G.M.; Joress, H.; Weihs, T. Enabling and controlling slow reaction velocities in low-density compacts of multilayer reactive particle. *Combustion and Flame* **2011**, *158*, 1084–1088.
7. Grieseler, R.; Au, I.S.; Kups, T.; Schaaf, P. Diffusion in thin bilayer films during rapid thermal annealing. *physica status solidi (a)* **2014**, *211, doi:*10.1002/pssa.201431039.